



United States Department of the Interior
U.S. Geological Survey
Geology, Energy & Minerals Science Center
MS 954 12201 Sunrise Valley Drive
Reston, VA 20192

November 10, 2023

MEMORANDUM

From: Paul C. Hackley, U.S. Geological Survey, Reston, Virginia, USA

To: Sandra Rodrigues, University of Queensland, Brisbane, Australia

Ref: data from Paleoproterozoic samples from McArthur Basin, Australia

Preamble: The data contained in this data package were collected according to the quality requirements of the U.S. Geological Survey (USGS) Energy and Minerals Mission Area Quality Management System, and have undergone secondary data review by a technical expert. However, the data have not been formally peer reviewed, nor approved for public release by the Director of the USGS. As such, the data are considered provisional and are subject to revision. Neither the USGS nor the United States Government may be held liable for any damages resulting from authorized or unauthorized data use. Data from this data package should be cited as follows: "Paul C. Hackley, written communication, 2023."

Sample Preparation and Analysis: Paleoproterozoic McArthur Basin samples (6) were received February 2019 in USGS-Reston as small core chips and a larger piece of slabbed core (sample LP3). Accompanying information included a proprietary report with thermal maturity and other information for the samples. Samples were sent to USGS for the express purpose of hydrous pyrolysis experiments to simulate petroleum generation from Paleoproterozoic rocks, for which the sample from the LP3 well was the only sample received in sufficient quantity.

Samples were crushed in a jaw crusher and sieved to obtain consistent size fractions. A representative aliquot passing 60 mesh (250 μm) was crushed to powder by hand using mortar and pestle. Rock powders were analyzed for total organic carbon (TOC) content at the USGS Petroleum Geochemistry Research Laboratory in Lakewood, Colorado, by LECO C744 carbon analyzer following carbonate removal at room temperature with 6 M HCl (Oliver and Warden, 2020). Programmed temperature pyrolysis at USGS-Lakewood used a Hydrocarbon Analysis with Kinetics (HAWK) instrument following typical procedures (Dreier and Warden, 2021). The geochemical screening analyses were determined according to the instrument manuals and included internal laboratory standards for all runs.

Samples containing TOC content >1.0 wt.% (4) were prepared for petrographic analysis in USGS-Reston from a representative aliquot passing 20 mesh (850 μm) according to ASTM D2797 (ASTM, 2021). Samples were imaged under oil immersion on a Leica DM 4000 microscope equipped with LED illumination and monochrome camera detection (QMS identity

Hilgers1) in white and blue incident light. Reflectance analyses were conducted according to ASTM D7708 (ASTM, 2023) using the computer program DISKUS-FOSSIL by Hilgers Technisches Buero with a YAG calibration standard (0.908% R_o) from Klein and Becker. The same 4 samples also were prepared as ultra-thin ($\sim 20\ \mu\text{m}$) sections for transmitted light petrographic analysis following standard procedures (Chaplin, 1998) and imaged on a Zeiss Axiomager microscope equipped with transmitted and incident light illumination.

Results: TOC content ranged <0.20 to $3.53\ \text{wt.}\%$ (Table 1). Sample LP3, which was the core slab intended for HP experiments, was split into 4 subsamples to obtain representative TOC content across the length of the core (Fig. 1).



Fig. 1. Photograph of sample LP3 sent to USGS for HP experiments, showing the rock fragments analyzed for TOC content and pyrolysis properties (labeled 1-4, see also Table 1).

Unfortunately, no intervals from the LP3 sample contained $>0.32\ \text{wt.}\%$ TOC, eliminating the possibility to use this sample for HP experiments. TOC content in samples from well 82-6 (Yalco Formation) ranged 0.67 to $1.70\ \text{wt.}\%$ whereas samples from well GRNT 79-5 [Barney Creek Formation, $\sim 1.64\ \text{Ga}$ depositional age (Page and Sweet, 1998)] ranged 2.09 to $3.53\ \text{wt.}\%$. The higher TOC ($3.53\ \text{wt.}\%$) and corresponding higher HI ($475\ \text{mg/g}$) in sample GRNT 79-5 195.88–195.95 m do indicate suitability for HP experiments to generate analyzable oil. This is further confirmed by low thermal maturity at the entrance to the oil window ($T_{\text{max}}\ 440^\circ\text{C}$). However, this sample was not provided in sufficient quantity to perform HP experiments, for which $>30\ \text{g}$ rock is needed. If sufficient quantities of rock material are still available from well GRNT 79-5 from samples with higher TOC content, these would be welcomed to try for experimental HP generation of analyzable oils.

Reflectance (of solid bitumen) analyses of the 4 rock samples with TOC content $>1.0\ \text{wt.}\%$ indicated immature values of 0.34 to 0.36% with high values of standard deviation (Table 1). The high standard deviation values are because the BRo measurements incorporated all types of solid bitumen included in the sample

(except from thucholite), including migrated material with void-filling textures and solid bitumen that is developing in situ from the thermal conversion of lamalginite and/or bituminite sensu Hackley et al. (2018).

USGS ID	Sample ID	Label	TOC	HI	OI	PI	S1	S2	S3	Tmax	BRo	s.d.	no.
E190206-001	82-6 88.09-88.13 m	na	0.67	92	25	0.03	0.02	0.62	0.17	434	nd	nd	nd
E190206-002	82-6 93.09-93.14 m	na	1.7	381	18	0.02	0.13	6.48	0.31	435	0.34	0.09	20
E190206-003	GRNT-79-5 177.77-177.86 m	na	2.09	410	12	0.06	0.51	8.56	0.25	438	0.36	0.11	37
E190206-004	GRNT-79-5 195.88-195.95 m	na	3.53	475	9	0.06	1.14	16.75	0.33	440	0.35	0.12	36
E190206-005	GRNT-79-5 237.70-237.85 m	na	3	415	10	0.06	0.77	12.42	0.29	441	0.35	0.08	26
E190206-006	LP3 Sample 19 413.74-413.94	1	<0.20	176	108	0.24	0.1	0.31	0.19	453	nd	nd	nd
E190206-006A	LP3 Sample 19 413.74-413.94A	2	0.28	156	75	0.17	0.09	0.44	0.21	455	nd	nd	nd
E190206-006B	LP3 Sample 19 413.74-413.94B	3	0.31	155	62	0.14	0.08	0.48	0.19	452	nd	nd	nd
E190206-006C	LP3 Sample 19 413.74-413.94C	4	0.32	169	81	0.21	0.14	0.54	0.26	452	nd	nd	nd

na, not applicable; nd, no data

Table 1. Data from the Paleoproterozoic McArthur Basin samples.

All four of the petrographically examined samples (from Yalco and Barney Creek formations) contain abundant lamalginite with strong fluorescence (Figs. 2–5). Fluorescence intensity was variable between individual lamella or within a single lamella in the same sample. Lamalginite has no contrast with the mineral matrix in reflected white light and is black to dark reddish in color. Lamalginite grades to fluorescent bituminite in some areas (where laminae are not apparent) and also develops a gray reflecting surface where thermally or otherwise converted to solid bitumen in some areas. Solid bitumen also occurs as a migratory phase and fills voids between authigenic minerals (Fig. 3 and Fig. 5). Typically, the migrated solid bitumen is non-fluorescent with higher reflectance whereas solid bitumen developing in situ from lamalginite retains some fluorescence and is lower reflectance. Some solid bitumen is patchy in appearance whereas some is homogeneous. These maceral descriptions for lamalginite, bituminite, and solid bitumen are consistent with modern literature descriptions (Hackley et al., 2018; Kus et al., 2017; Pickel et al., 2017) and conform to recently presented petrographic descriptions for the Barney Creek Formation (Li et al., 2023). Moreover, the thermal maturity data herein also conform to that presented in Li et al. (2023) and indicate immature or early mature conditions.

The lamalginite present in all four of the petrographically examined samples is typical of lacustrine microbial mat textures. In contrast to more organic-rich microbialites, e.g., Eocene Green River Mahogany zone (Hackley et al., 2017), the McArthur Basin samples contain discrete organic-rich lamella of 5–10 μm thickness, separated by minerals (authigenic and detrital). Lamalginite folds over authigenic carbonates in many instances (Figs. 2–5), a texture suggestive of microbially induced mineralization and the presence of a cohesive biofilm of extracellular polymeric substances (Wingender et al., 1999). The observation of organic-rich microbialite textures is consistent with prior petrographic observations from Crick et al. (1988) who described fluorescent lamalginite from Paleoproterozoic McArthur Basin samples. A microbialite origin also is consistent with work by French et al. (2020) who observed that methylhopane and carotenoid signatures in the Barney Creek were characteristic of saline

lacustrine organic matter, although see Kunzmann et al. (2019) who suggested a marine environment based on sedimentological associations.

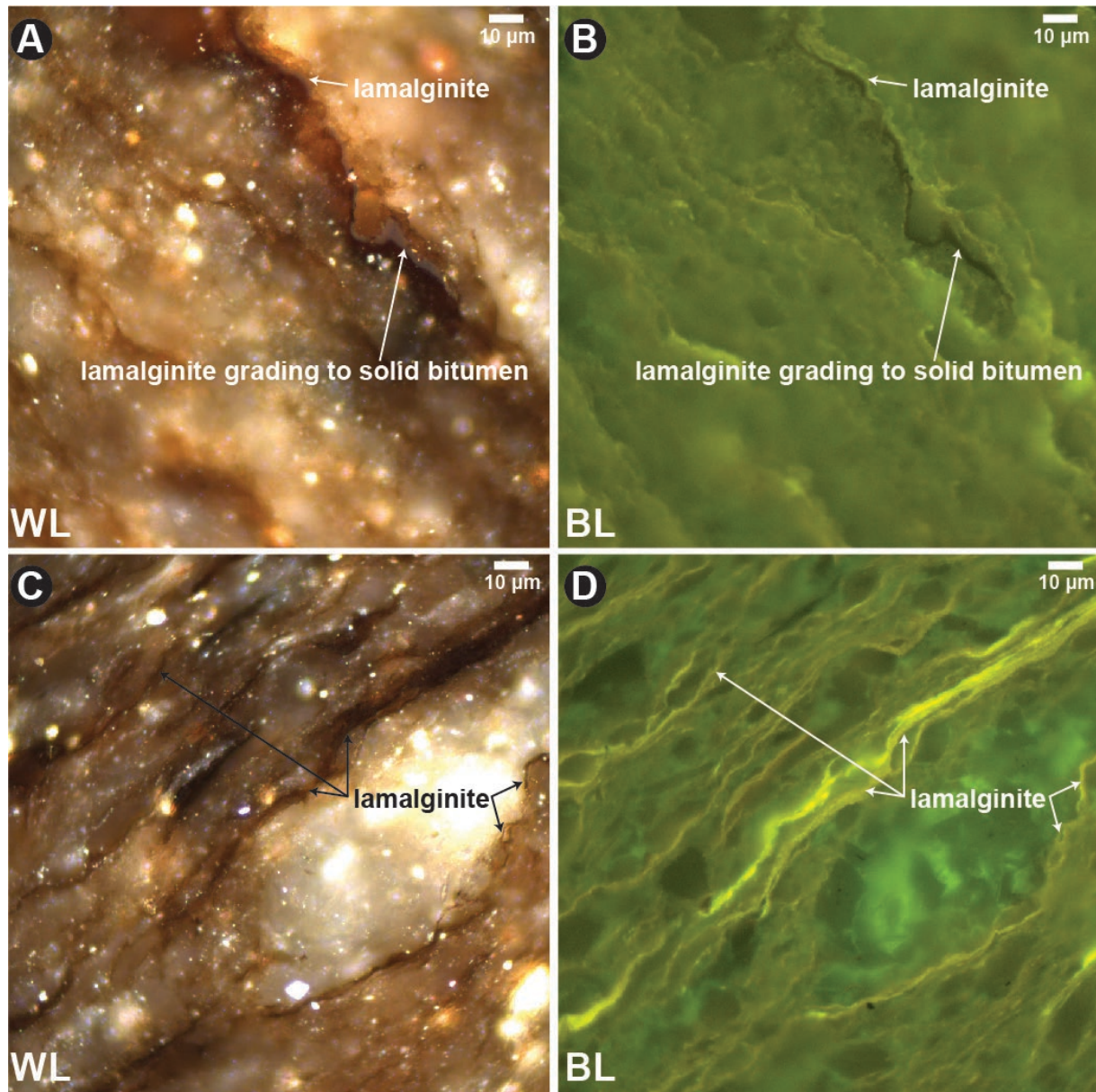


Fig. 2. Organic matter in the Paleoproterozoic Yalco Formation (sample 82-6 93.09 m). A. White light (WL) under oil immersion. B. Same field as A under blue light (BL) fluorescence. C. White light under oil immersion. D. Same field as C under blue light fluorescence.

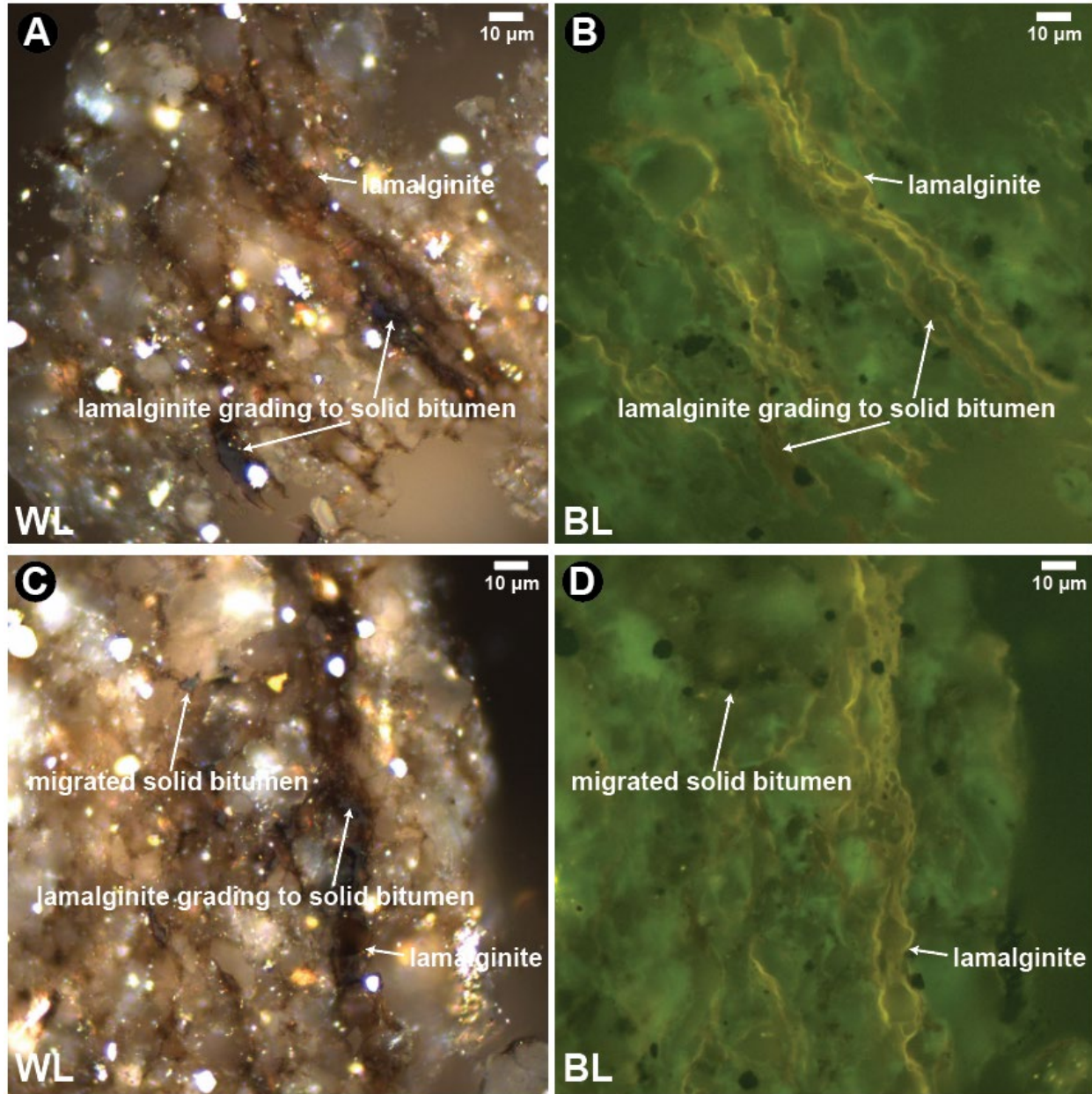


Fig. 3. Organic matter in the Paleoproterozoic Barney Creek Formation (sample GRNT-79-5 177.77–177.86 m). A. White light (WL) under oil immersion. B. Same field as A under blue light (BL) fluorescence. C. White light under oil immersion. D. Same field as C under blue light fluorescence.

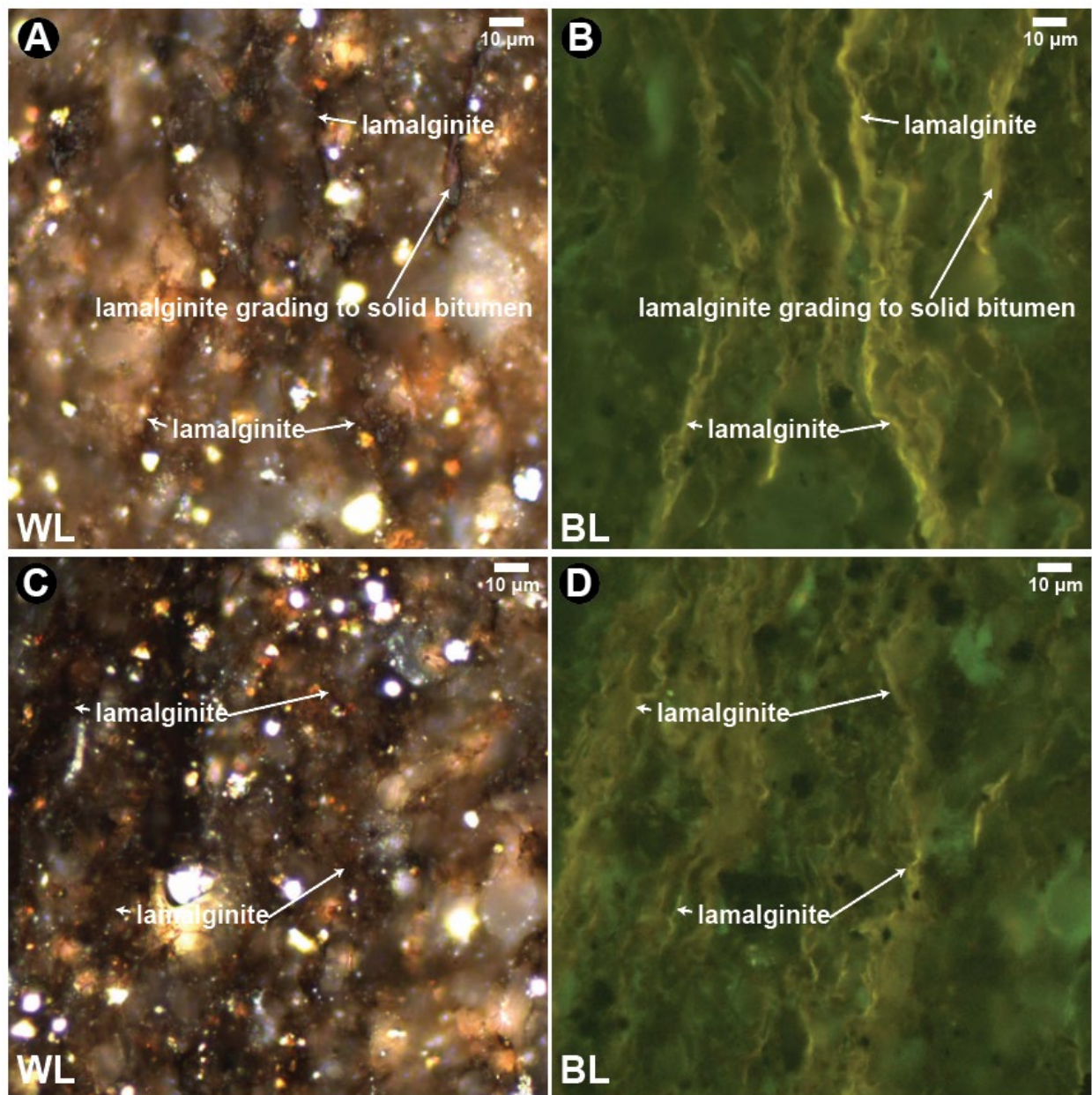


Fig. 4. Organic matter in the Paleoproterozoic Barney Creek Formation (sample GRNT-79-5 195.88–195.95 m). A. White light (WL) under oil immersion. B. Same field as A under blue light (BL) fluorescence. C. White light under oil immersion. D. Same field as C under blue light fluorescence.

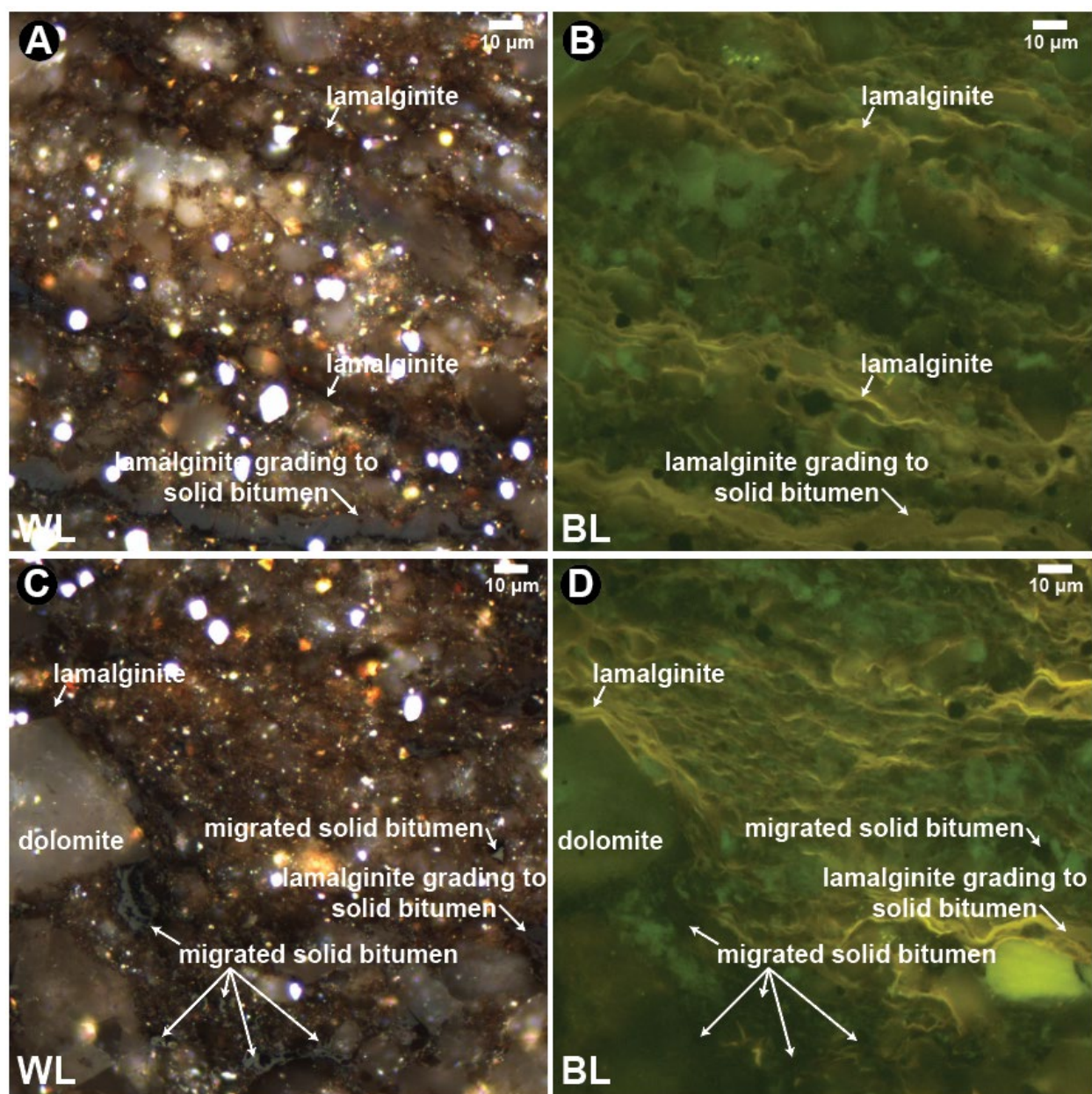


Fig. 5. Organic matter in the Paleoproterozoic Barney Creek Formation (sample GRNT-79-5 237.70–237.85 m). A. White light (WL) under oil immersion. B. Same field as A under blue light (BL) fluorescence. C. White light under oil immersion. D. Same field as C under blue light fluorescence.

The sample from 237.70–237.85 m in well GRNT-79-5 was selected for a scanning electron microscopy-cathodoluminescence (SEM-CL) study on the basis of its strong organic fluorescence. However, strongly fluorescent lamalginite in this sample does not exhibit an imageable SEM-CL response (Fig. 6), using the equipment and measurement conditions currently available at USGS. This is speculatively attributed to radiolytic alteration, based on the observation that CL intensity in other strongly fluorescent samples (from other formations apart

from this Paleoproterozoic sample set) seems to follow an almost one-to-one correspondence to fluorescence intensity (Hackley et al., submitted). However, lack of CL response in the Barney Creek sample could also be due to differences in the original molecular structure of its organic matter or differences in the diagenetic conditions that it experienced.

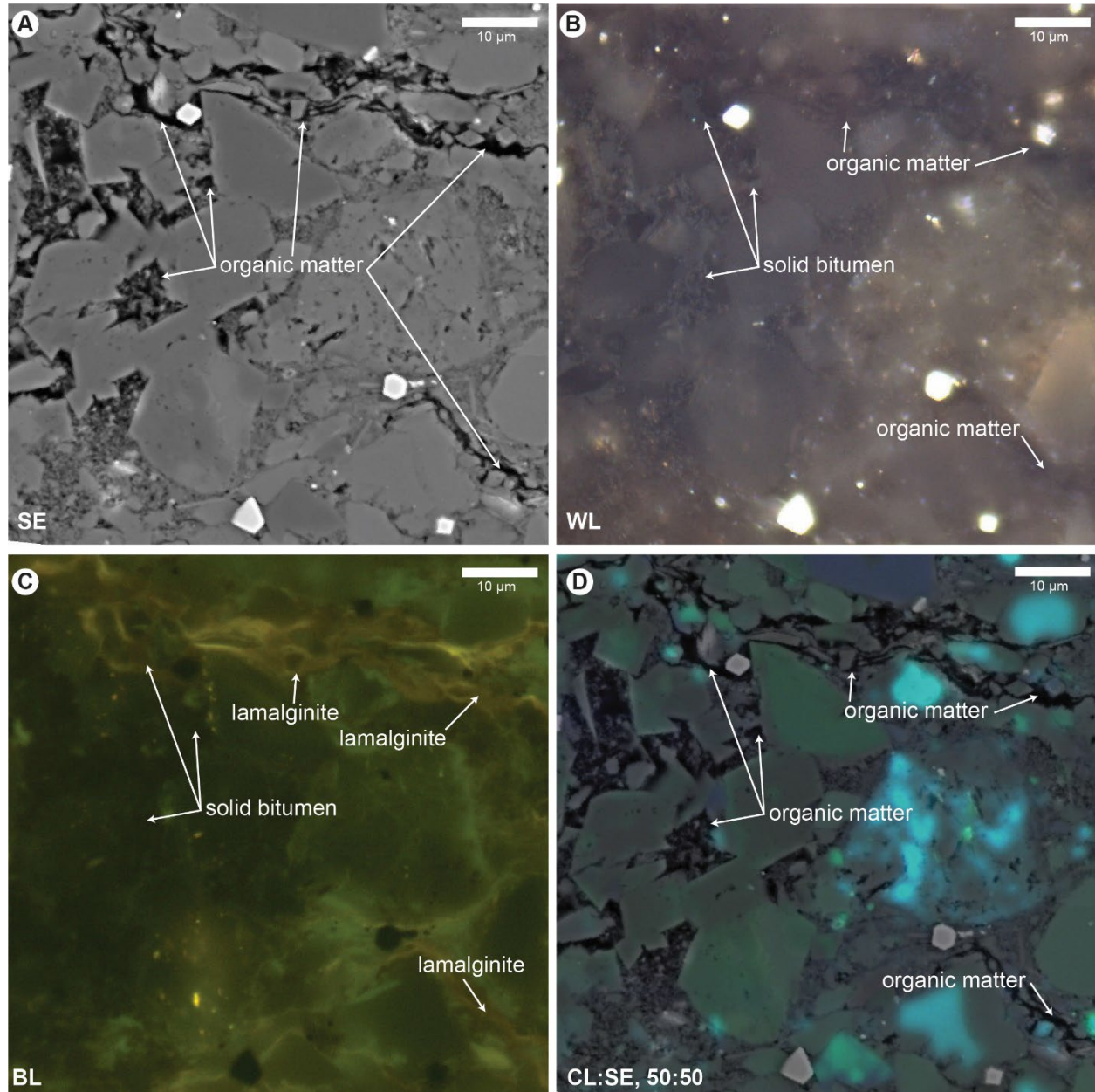


Fig. 6. Organic matter in the Paleoproterozoic Barney Creek Formation (sample GRNT-79-5 237.70–237.85 m). A. Secondary electron (SE) image. B. Same field as A under white light (WL). C. Same field as A-B under blue light (BL) fluorescence. D. Same field as A-C under 50:50 cathodoluminescence [CL, note red channel is not shown due to streaking from long lifetime luminescence (phosphorescence) from carbonates and/or apatite] and SE overlay.

Observations from thin sections confirm the organic petrography information from polished pellets and provide additional insights on mineralogy in the 4 samples with TOC >1.0 wt.%. In the Yalco Formation sample from well 82-6 93.09 m, detrital quartz, muscovite, and rare microcline and biotite are matrix-supported in fine-grained clays, quartz and plagioclase. Lamalginite wraps around sparse ovoid pyrite nodules (Fig. 7).

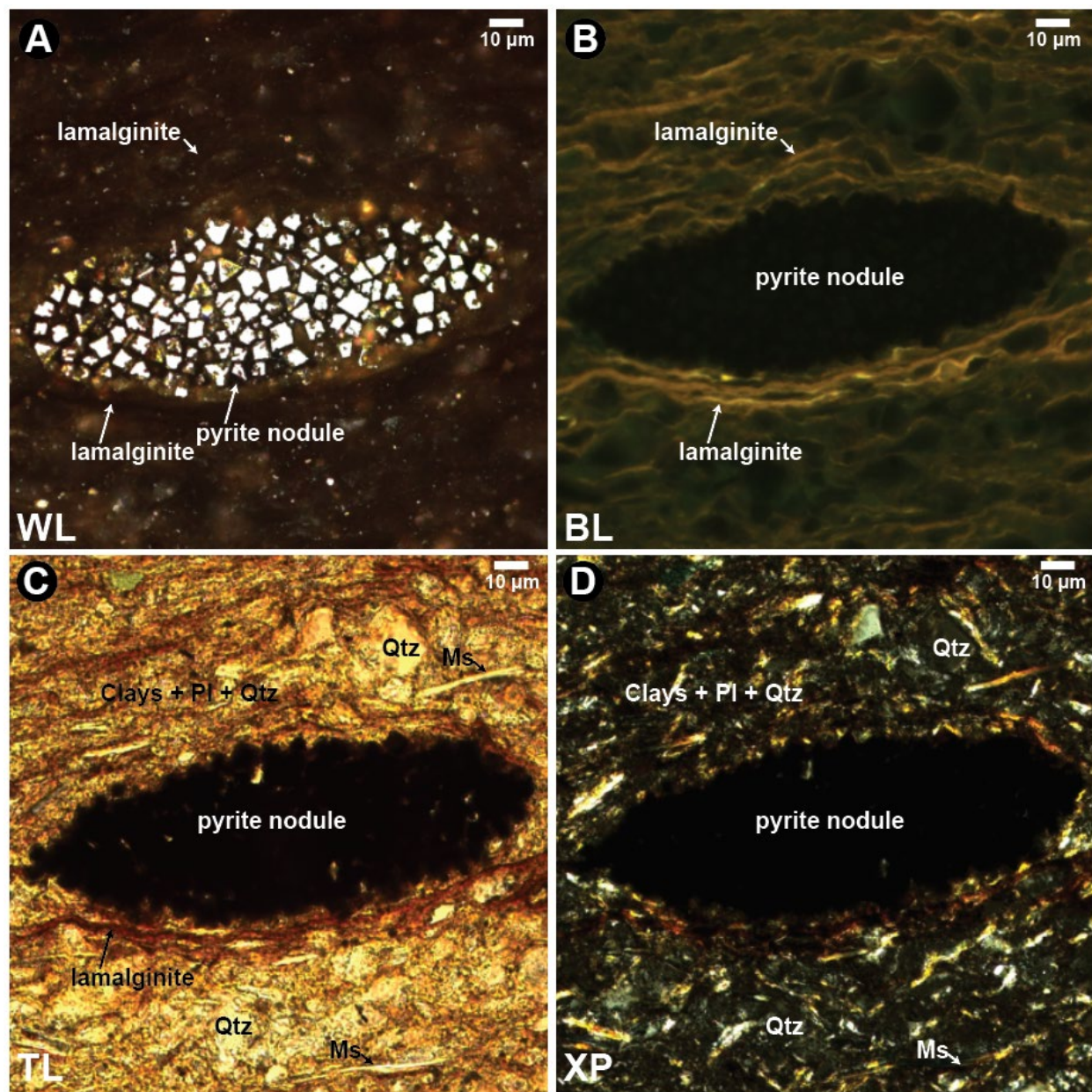


Fig. 7. Organic matter and minerals in the Paleoproterozoic Yalco Formation (sample 82-6 93.09 m). A. White light (WL) under oil immersion. B. Same field as A under blue light (BL) fluorescence. C. Same field as A-B in plane-polarized transmitted light (TL). D. Same field as A-C in cross-polarized (XP) transmitted light. Mineral abbreviations after Kretz (1983): Qtz, quartz; Ms, muscovite; Pl, plagioclase.

Samples from the GRNT-79-5 well also contain detrital matrix-supported muscovite and quartz in fine-grained clay, quartz, and feldspars (Fig. 8).

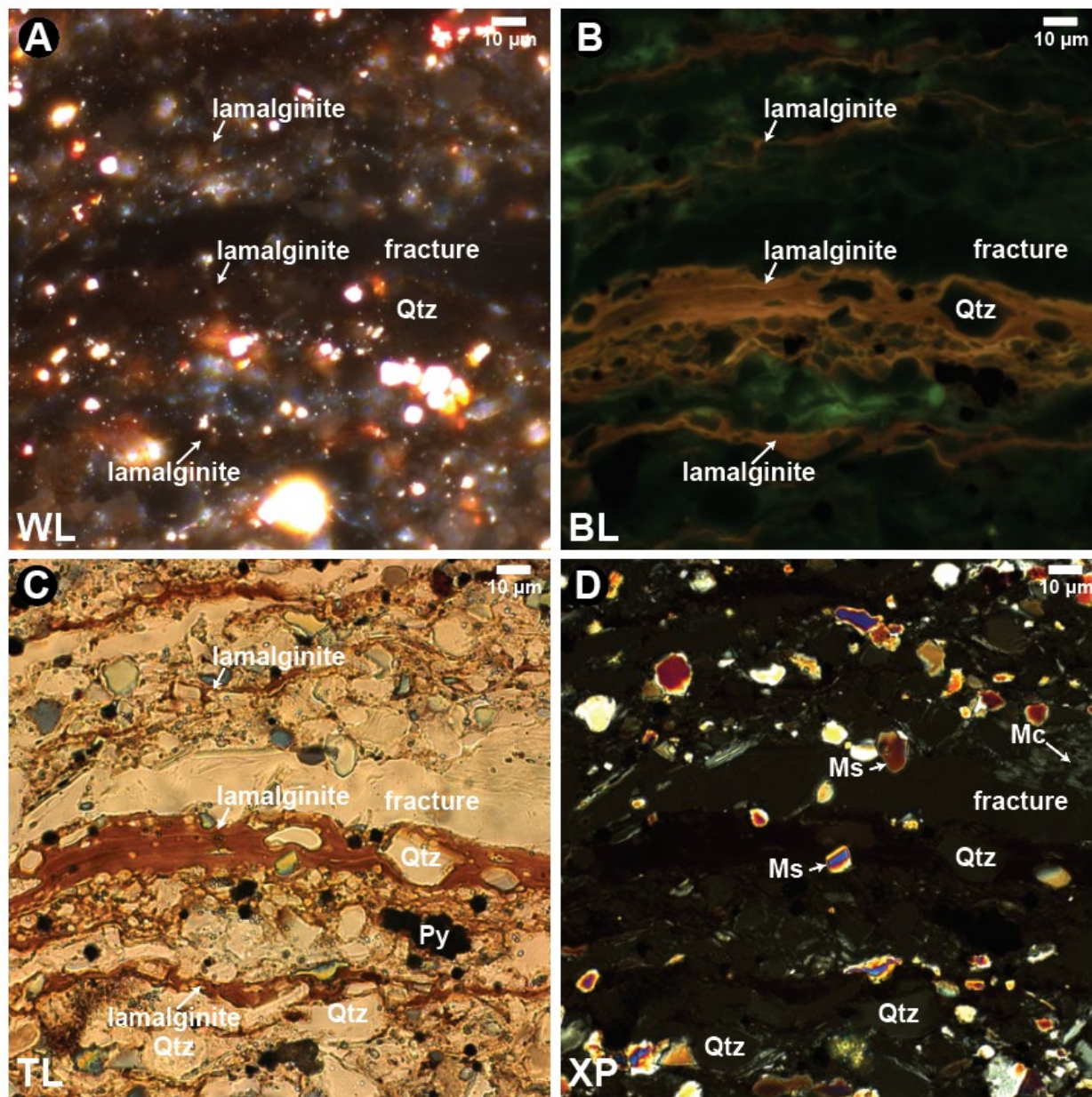


Fig. 8. Organic matter and minerals in the Paleoproterozoic Barney Creek Formation (sample GRNT-79-5 177.77–177.86 m). A. White light (WL) under oil immersion. B. Same field as A under blue light (BL) fluorescence. C. Same field as A-B in plane-polarized transmitted light (TL). D. Same field as A-C in cross-polarized (XP) transmitted light. Mineral abbreviations after Kretz (1983): Qtz, quartz; Ms, muscovite; Mc, microcline; Py, pyrite.

The samples from GRNT-79-5 177.77–177.86 and 195.88–195.95 m also contain abundant sulfides, and, in some zones, sulfide is oxidized at its rims, possibly suggesting hydrothermal fluid alteration. Also present in GRNT-79-5 177.77–177.86 m is matrix-supported pristine tabular

euohedral plagioclase with albite twinning, supporting a volcanogenic origin, and rare alkali feldspar. Matrix supported carbonate (presumably dolomite) is present in sample GRNT-79-5 195.88-195.95 m (Fig. 9).

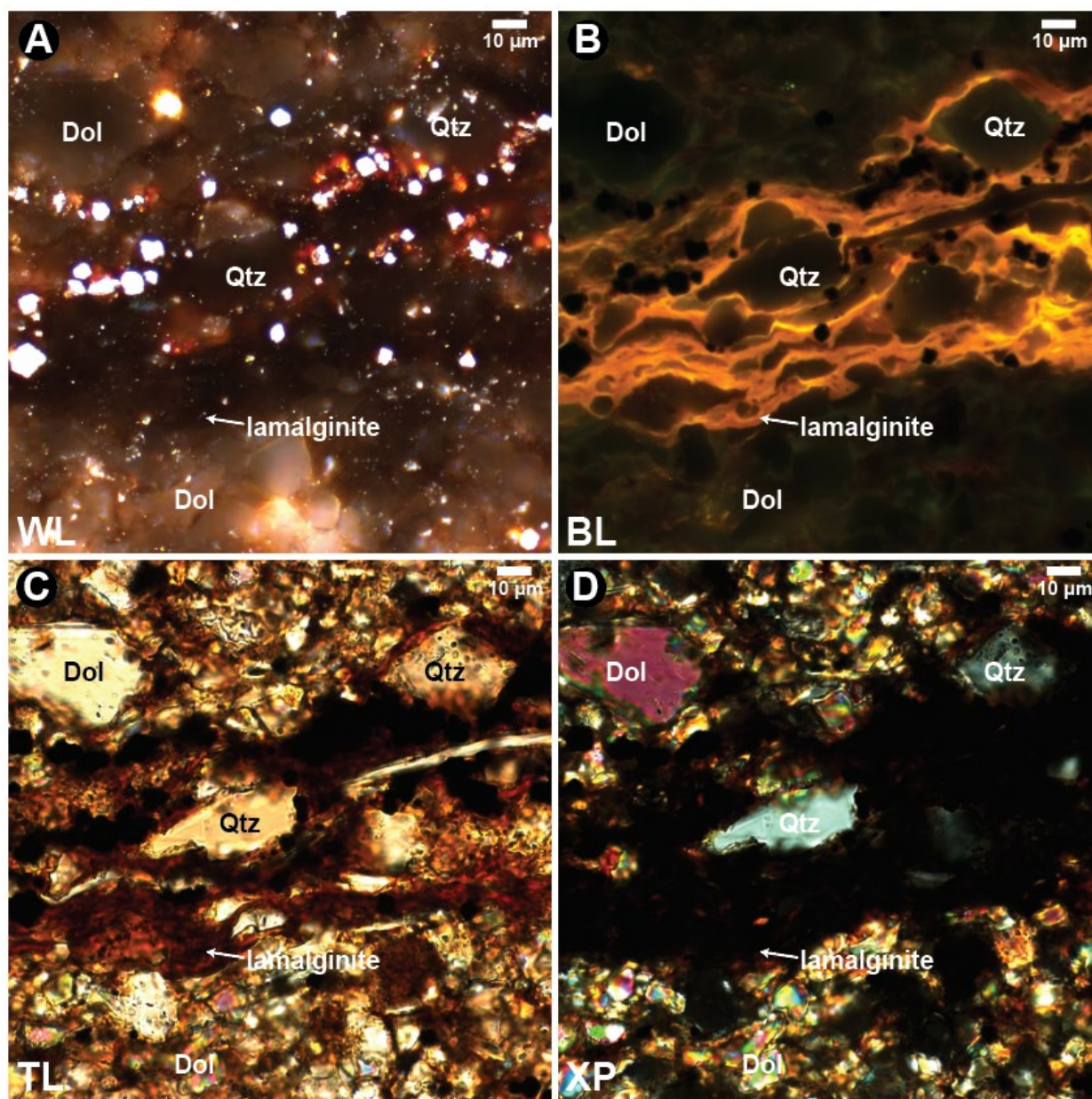


Fig. 9. Organic matter and minerals in the Paleoproterozoic Barney Creek Formation (sample GRNT-79-5 195.88-195.95 m). A. White light (WL) under oil immersion. B. Same field as A under blue light (BL) fluorescence. C. Same field as A-B in plane-polarized transmitted light (TL). D. Same field as A-C in cross-polarized (XP) transmitted light. Mineral abbreviations after Kretz (1983): Qtz, quartz; Dol, dolomite.

The sample from GRNT-79-5 237.70-237.85 m contains alternating darker clay-rich lamella which contain a greater proportion of organic matter and lighter carbonate rich layers (Fig. 10).

Quartz, muscovite, and carbonate are commonly matrix supported in the clay-rich layers. Thucholite appears to be present only in the clay-rich layers. Carbonate throughout both clay-rich and carbonate-rich layers is frequently rhombohedral, indicating an authigenic origin. Similar to all other observations of lamalginite, fold-overs on carbonate are common, indicating contemporaneous formation in a microbial mat environment. A rare carbonate ovoid in sample GRNT-79-5 237.70-237.85 m (Fig. 10) may indicate local development of concretions but this was a singular observation.

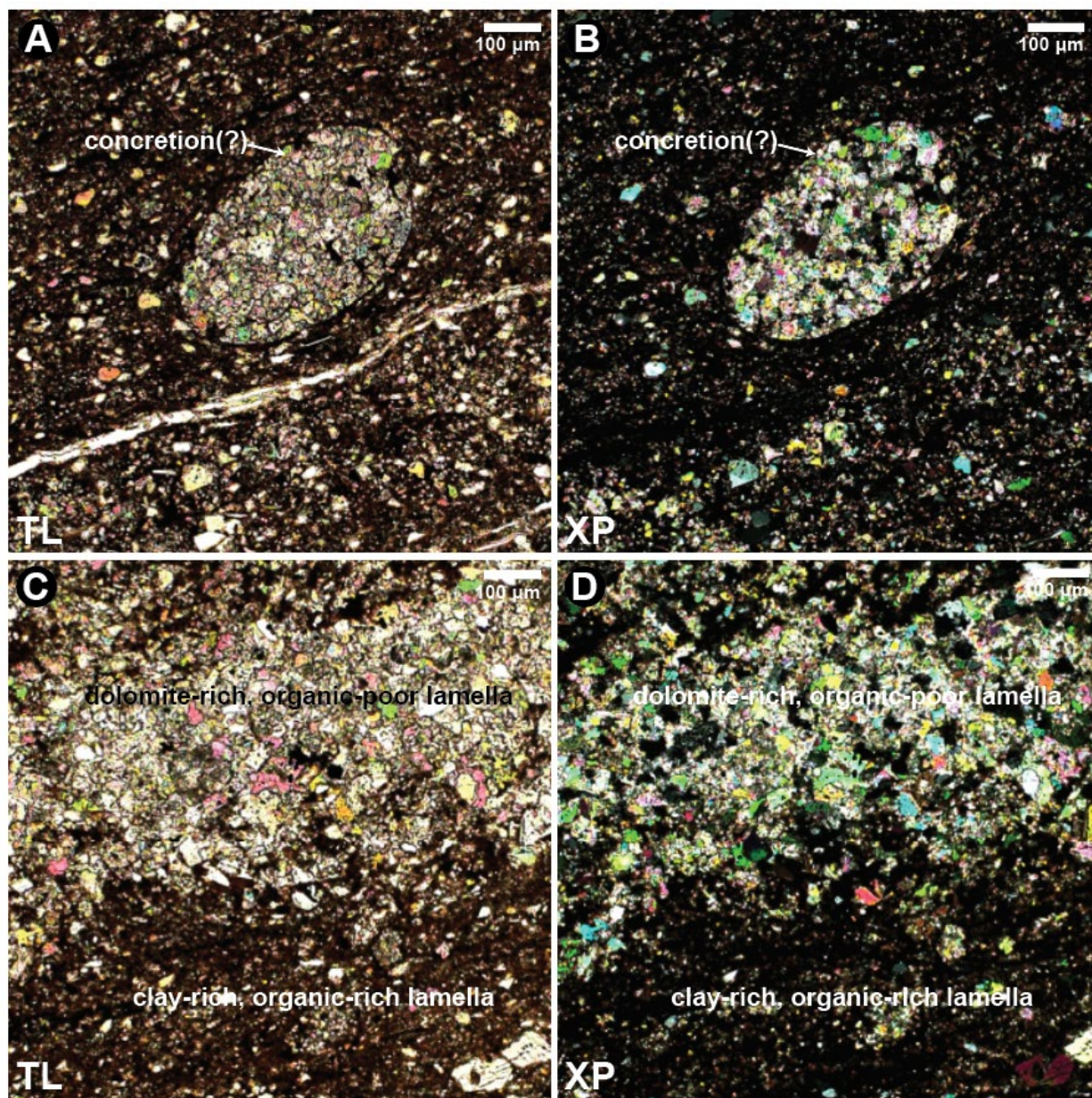


Fig. 10. Organic matter and minerals in the Paleoproterozoic Barney Creek Formation (sample GRNT-79-5 237.70-237.85 m). A. Plane-polarized transmitted light (TL). B. Same field as A in cross-polarized (XP) transmitted light. C. Plane-polarized transmitted light (TL). D. Same field as C in cross-polarized (XP) transmitted light.

Thucholites are common in samples from 177.77–177.86 m (Fig. 11) and 237.70–237.85 m. Thucholite in the Barney Creek was also noted by Crick et al. (1988). Lamalginite appears to wrap around thucholite (e.g., Khan et al., 2020) as well as to be of the same optical character [similar reflectance and contrast to mineral matrix (Fig. 11A), similar fluorescence color and intensity (Fig. 11B), similar color and opacity in transmitted light (Fig. 11C), and similar isotropy in crossed polars (Fig. 11D)] at the thucholite margins. These observations are true only at the margins of thucholite, whereas in thucholite centers, the reflectance is higher than lamalginite (Fig. 11A), fluorescence intensity is lower (Fig. 11B), and opacity is higher (Fig. 11C).

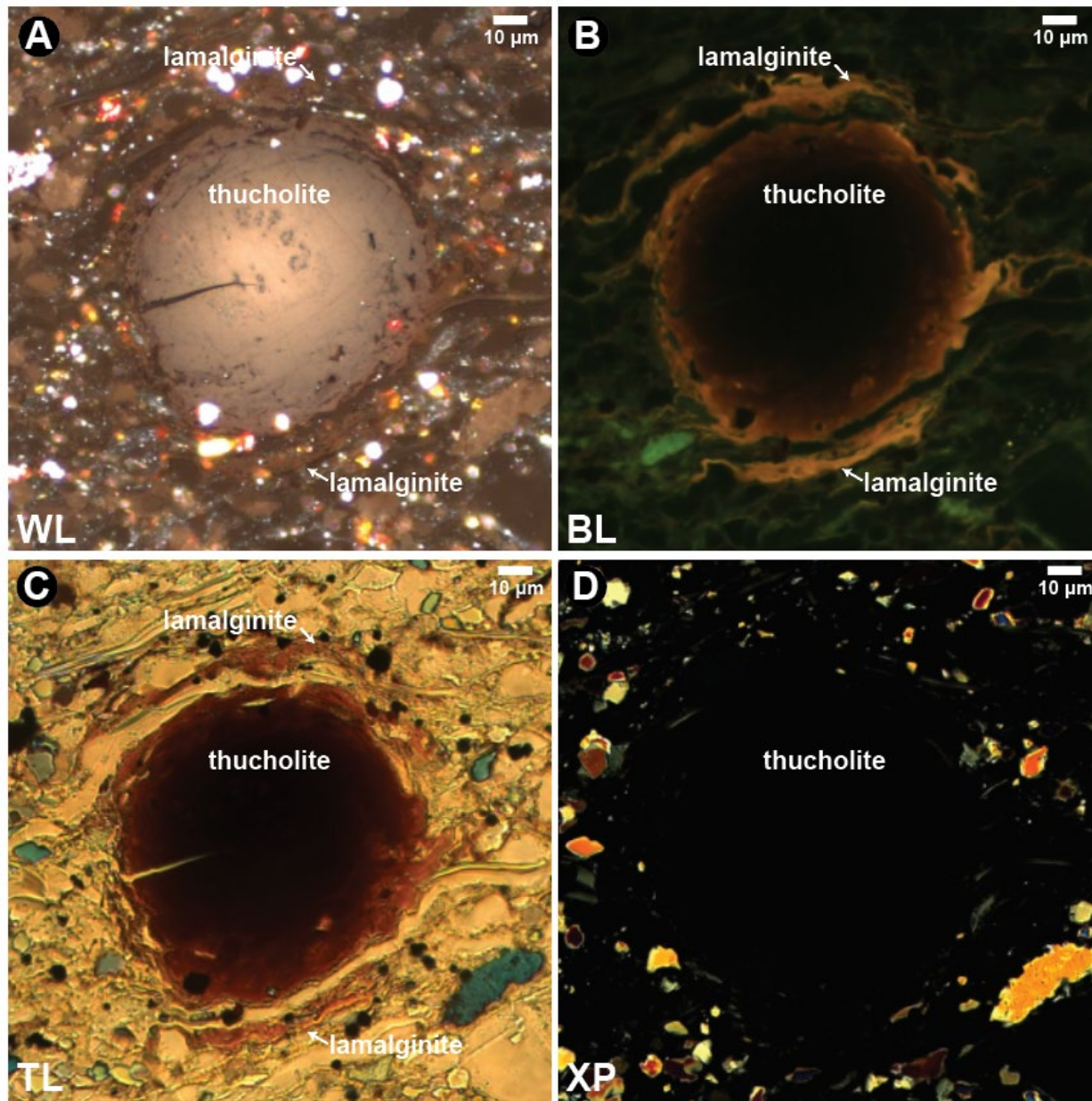


Fig. 11. Thucholite in the Paleoproterozoic Barney Creek Formation (sample GRNT-79-5 177.77–177.86 m). A. White light (WL) under oil immersion. B. Same field as A under blue light

(BL) fluorescence. C. Same field as A-B in plane-polarized transmitted light (TL). D. Same field as A-C in cross-polarized (XP) transmitted light.

The observation of lamalginite lamellae wrapping thucholite (and pyrite nodules, see above) indicates thucholite/pyrite nodule formation and hardening occurred during early diagenesis contemporaneous with induration. Speculatively, this texture could indicate early immobilization and mechanical stiffening of organic matter by radiolytic alteration in the immediate vicinity (i.e., within ~50 μm) of the ionizing radiation source. The contemporaneous nature of thucholite development and early diagenesis/induration indicates ‘geologically instantaneous’ development of the higher reflectance internal areas of the thucholite, and suggests its aromaticity will be different than solid bitumen of equivalent reflectance that is matured through burial metamorphism (Schito et al., 2023). Radial fractures in thucholite (Fig. 11) probably occur due to shrinkage of the hardening thucholite, which occurs during crosslinking induced by radiolytic alteration, i.e., the molecular structure condenses and its specific volume decreases (Charlesby, 1954). The radial fractures are wedge-shaped opening toward the outer circumference of the thucholite due to a proportional increase in shrinkage (Rasmussen and Glover, 1990). Most workers have inferred thucholite development in organic-rich shale occurs via polymerization of surrounding organic matter caused by ionizing radiation from a central radioactive mineral (Khan et al., 2020; Luo et al., 2014; Zheng et al., 2021). However, if this were always the case, there should be no continuity from thucholite organic matter to lamellar organic matter in the matrix. Therefore, the contiguous nature of some Barney Creek lamalginite with organic matter at the margins of thucholite (e.g., right side of thucholite in Fig. 11B) requires further investigation.

Future Studies: Some suggestions for future studies using the current sample set (or additional, related materials) are the following:

1. Using an appropriate sample (>30 g, high TOC, low maturity, e.g., GRNT-79-5 237.70–237.85 m), generate analyzable quantities of oils which could be compared to sampled oils (if any are available) in the McArthur Basin. The composition of the artificially generated oil also could be used to predict compositions of yet-to-be sampled naturally produced oils which would be found where similar McArthur Basin source rock is mature for petroleum generation.
2. Using LA-ICP-MS, compare compositions of thucholites to inorganic matrix and lamalginite to test the hypothesis that the thucholite forms over the matrix material. This work can be done in-house at USGS by broadening our collaboration to additional partners. This work potentially could be extended to dating the timing of thucholite formation through radiogenic isotope measurements, e.g., Re-Os, U-Pb, Lu-Hf. Or, using SEM, compare matrix inclusions in thucholite to inclusions in contiguous organic-rich lamella. This work also could be done in-house at USGS by broadening our collaboration to additional partners.
3. Using Raman spectroscopy, compare aromaticity (i.e., Raman parameters D1/G, RBS, etc.) of thucholite to similar reflectance solid bitumen from burial metamorphism, to test the hypothesis that aromaticity development from radiolytic decay is dissimilar, i.e., heating rate controls aromaticity development (Schito et al., 2023; Song et al., 2023).

Similar work has not been done using thucholite to my knowledge. This work also could be done in-house at USGS by broadening our collaboration to additional partners.

References

- ASTM, 2021. D2797 Standard practice for preparing coal samples for microscopical analysis by reflected light, Petroleum products, lubricants, and fossil fuels; Gaseous fuels; coal and coke, sec. 5, v. 05.06. ASTM International, West Conshohocken, PA, <https://www.astm.org/Standards/D2797.htm>.
- ASTM, 2023. D7708 Standard test method for microscopical determination of the reflectance of vitrinite dispersed in sedimentary rocks, Petroleum products, lubricants, and fossil fuels; Gaseous fuels; coal and coke, sec. 5, v. 05.06. ASTM International, West Conshohocken, PA, <https://www.astm.org/Standards/D7708.htm>.
- Chaplin, I., 1998. Preparation of thin sections. *Microscopy Today* 6, 8–9.
- Charlesby, A., 1954. The cross-linking and degradation of paraffin chains by high-energy radiation. *Royal Society of London Proceedings, ser. A* 222, 60–74.
- Crick, I.H., Boreham, C.J., Cook, A.C., Powell, T.G., 1988. Petroleum geology and geochemistry of Middle Proterozoic McArthur Basin, northern Australia II: assessment of source rock potential. *AAPG Bulletin* 72, 1495–1514.
- Dreier, M., Warden, A., 2021. Petroleum Geochemistry Research Laboratory Programmed Pyrolysis Method. U.S. Geological Survey, U.S. Geological Survey webpage.
- French, K.L., Birdwell, J.E., Vanden Berg, M.D., 2020. Biomarker similarities between the saline lacustrine Eocene Green River and the Paleoproterozoic Barney Creek Formations. *Geochimica et Cosmochimica Acta* 274, 228–245.
- Hackley, P.C., McAleer, R.J., Jubb, A.M., Valentine, B.J., Birdwell, J.E., submitted. Cathodoluminescence differentiates sedimentary organic matter types. *Scientific Reports*.
- Hackley, P.C., Valentine, B.J., Hatcherian, J.J., 2018. On the petrographic distinction of bituminite from solid bitumen in immature to early mature source rocks. *International Journal of Coal Geology* 196, 232–245.
- Hackley, P.C., Valentine, B.J., Voortman, L.M., Van Oosten Slingeland, D.S.B., Hatcherian, J., 2017. Utilization of integrated correlative light and electron microscopy (iCLEM) for imaging sedimentary organic matter. *Journal of Microscopy* 267, 371–383.
- Khan, I., Zhong, N., Luo, Q., Ai, J., Yao, L., Luo, P., 2020. Maceral composition and origin of organic matter input in Neoproterozoic–Lower Cambrian organic-rich shales of Salt Range Formation, upper Indus Basin, Pakistan. *International Journal of Coal Geology* 217, 103319.

- Kretz, R., 1983. Symbols for rock-forming minerals. *American Mineralogist* 68, 277–279.
- Kunzmann, M., Schmid, S., Blaikie, T.N., Halverson, G.P., 2019. Facies analysis, sequence stratigraphy, and carbon isotope chemostratigraphy of a classic Zn-Pb host succession: The Proterozoic middle McArthur Group, McArthur Basin, Australia. *Ore Geology Reviews* 106, 150–175.
- Kus, J., Araujo, C.V., Borrego, A.G., Flores, D., Hackley, P.C., Hámor-Vidó, M., Kalaitzidis, S., Kommeren, C.J., Kwiecińska, B., Mastalerz, M., Mendonça Filho, J.G., Menezes, T.R., Misz-Kennan, M., Nowak, G.J., Petersen, H.I., Rallakis, D., Suárez-Ruiz, I., Sýkorová, I., Životić, D., 2017. Identification of alginite and bituminite in rocks other than coal. 2006, 2009, and 2011 round robin exercises of the ICCP Identification of Dispersed Organic Matter Working Group. *International Journal of Coal Geology* 178, 26–38.
- Li, S., Wang, X., Hu, M.-Y., 2023. Organic matter accumulation and hydrothermal effect of the Barney Creek formation in the Glyde Sub-basin, northern Australia. *Geoenergy Science and Engineering* 230, 212216.
- Luo, Q., Zhong, N., Qin, J., Li, K., Zhang, Y., Wang, Y., Ma, L., 2014. Thucholite in Mesoproterozoic shales from northern north China: Occurrence and indication for thermal maturity. *International Journal of Coal Geology* 125, 1–9.
- Oliver, T., Warden, A., 2020. Petroleum Geochemistry Research Laboratory Total Organic Carbon and Total Carbon Method. U.S. Geological Survey, U.S. Geological Survey webpage.
- Page, R.W., Sweet, I.P., 1998. Geochronology of basin phases in the western Mt Isa Inlier, and correlation with the McArthur Basin. *Australian Journal of Earth Sciences* 45, 219–232.
- Pickel, W., Kus, J., Flores, D., Kalaitzidis, S., Christanis, K., Cardott, B.J., Misz-Kennan, M., Rodrigues, S., Hentschel, A., Hamor-Vido, M., Crosdale, P., Wagner, N., 2017. Classification of liptinite – ICCP System 1994. *International Journal of Coal Geology* 169, 40–61.
- Rasmussen, B., Glover, J.E., 1990. The diagenetic and economic significance of composite grains of monazite and hydrocarbon in Western Australian arenites. *Journal of the Geological Society of London* 147, 843–850.
- Schito, A., Muirhead, D., Parnell, J., 2023. Towards a kerogen-to-graphite kinetic model by means of Raman spectroscopy. *Earth Science Reviews* 237, 104292.
- Song, J., Hackley, P.C., Sanders, M.M., Jubb, A.M., Luo, Q., 2023. Thermal evolution of graptolite and solid bitumen properties at high maturity under natural and artificial conditions. *International Journal of Coal Geology* 273, 104269.
- Wingender, J., Neu, T.R., Flemming, H.-C., 1999. What are bacterial extracellular polymeric substances?, in: Wingender, J., Neu, T.R., Flemming, H.-C. (Eds.), *Microbial*

Extracellular Polymeric Substances: Characterization, Structure and Function. Springer-Verlag, Berlin Heidelberg, pp. 1–19.

Zheng, X., Schovsbo, N.H., Bian, L., Luo, Q., Zhong, N., Rudra, A., Goodarzi, F., Sanei, H., 2021. Alteration of organic macerals by uranium irradiation in lower Paleozoic marine shales. *International Journal of Coal Geology* 239, 103713.